Received: 27 June 2018 | Revised: 17 September 2018 | Accepted: 16 October 2018

DOI: 10.1002/mrm.27598

FULL PAPER

Magnetic Resonance in Medicine

Cerebrospinal fluid–suppressed T_2-weighted MR imaging at 7 T for human brain

Jullie W. Pan | **Chan Hong Moon** | **Hoby P. Hetherington**

Magnetic Resonance Research Center, Department of Radiology, University of Pittsburgh, Pittsburgh, Pennsylvania

Correspondence
Jullie W. Pan, Magnetic Resonance Research Center, Department of Radiology, University of Pittsburgh, Pittsburgh, PA 15213.
Email: jwp44@pitt.edu

Funding information
NIH; Grant/Award numbers R01EB011639, R01NS090417, R01NS081772 and R01EB024408. We thank Tiejun Zhao and Tobias Kober, Siemens Medical Systems for advice. Thanks also to Mark Lowe and Ken Sakaie, Cleveland Clinic Foundation for review of their 7T T2 parameters.

Purpose: T_2-weighted lesional imaging is most commonly performed using inversion recovery turbo spin echoes. At 7 T, however, this acquisition is limited for specific absorption rate and resolution. This work describes and implements a method to generate CSF-suppressed T_2-weighted imaging.

Methods: The strategy uses a driven equilibrium spin-echo preparation within an inversion recovery with multiple 3D gradient-echo imaging blocks. Images are combined using the self-normalization approach, which achieves CSF suppression through optimized timing of individual blocks and minimizes sources of variation due to coil receptivity, T_2^*, and proton density. Simulations of the magnetization-prepared fluid-attenuated inversion recovery gradient-echo (MPFLAGRE) method over T_1 and T_2 relaxation values are performed, and in vivo demonstrations using an 8×2 transceiver array in healthy controls are shown.

Results: The specific absorption rate of the calculated MPFLAGRE sequence is 11.1 ± 0.5 W ($n = 5$ volunteers), which is $74 \pm 2\%$ of the US Food and Drug Administration guidelines. This method acquires both contrasts for CSF suppression with detection of long T_2 components and T_2-weighted imaging in a single acquisition. In healthy controls, the former contrast generates increased signal in the cortical rim and ependyma. A comparison is shown with a conventional 3D SPACE fluid-attenuated inversion recovery acquisition, and sensitivity to pathology is demonstrated in an epilepsy patient.

Conclusion: As applied with the 8×2 transceiver, the MPFLAGRE sequence generates both whole-brain contrast suitable for lesional and T_2-weighted imaging at 7 T in fewer than 10 minutes within the US Food and Drug Administration's specific absorption rate guidelines.

KEYWORDS
7T, FLAIR, MP2RAGE, SAR, T_2 weighted

1 | INTRODUCTION

The increase in SNR at 7 T relative to 3 T has been used by numerous groups for higher-accuracy physiological and metabolic MRI.[1-3] However, although high-resolution T_1-weighted structural imaging has been applied quickly,[4,5] T_2-weighted and fluid attenuated inversion recovery (FLAIR) imaging at 7 T has been less implemented—most likely

because of the increased power deposition and poor transmit homogeneity due to the need for multiple spin echoes. Parallel transmit arrays have mitigated inhomogeneity problems; for example, RF shimming and a dual-row transceiver array can achieve 15% SD B_1^+ over the human brain (Supporting Information Figures S1 and S2).[6] However, given the squared dependence of voltage with frequency at 7 T, [7] turbo spin-echo acquisitions or the use of adiabatic pulses still result in high specific absorption rate (SAR), such that T_2-weighted imaging covering the entire brain in acceptable scan times remains challenging. The variable flip angle turbo spin-echo sequence provides a reasonable solution to control power deposition; however, it is sensitive to B_1^+ inhomogeneity,[8-11] with several groups proposing design of parallel transmit pulses as a function of k-space position to generate more homogeneous excitation and inversion profiles. With this approach for turbo spin echo, however, achieving consistent contrast and motion insensitivity can be problematic by virtue of the dependence on accurate B_1^+ maps and applied B_1 variation between k-points.[8,12] Alternatively, to altogether avoid multiple refocusing pulses, a driven equilibrium spin-echo strategy to longitudinally encode T_2 contrast (i.e., T_2 preparation) has been useful.[13-15] To reduce the sensitivity of the acquisition to B_1^+ inhomogeneity at 7 T, Dyvorne and Balchandani[16] implemented the T_2 preparation with an adiabatic spin-echo module in a multislab approach to generate excellent T_2-weighted whole-brain coverage at 0.8-mm^3 isotropic resolution (approximate 5.5-minute acquisition). The FLAIR imaging at 7 T, however, remains challenging.

To suppress the CSF signal, the now commonly used calculated MP2RAGE images from Marques[17] provides an insightful T_1-based approach. This self-correcting normalization combines 2 images acquired at different delays after an inversion to give a calculated signal within the range of [–0.5, 0.5]. With a reconstruction in the complex domain (Eq. 1),[17] the calculated signal retains sensitivity to the inversion recovery, while eliminating B_0-based T_2^* phase effects and correcting for common factors of M_0 and B_1^-. Inspection of this reconstruction shows that the largest signal (+0.5) is seen when the intensities between the 2 images are equal, and the smallest signal (–0.5) when the intensities are equal and inverted in sign. For CSF, the calculated signal returns in the negative range (–0.5 to 0), whereas the white matter (WM) and gray matter (GM) return in the positive range (0 to +0.5). In the MP2RAGE acquisition, the sign and timings of the individual imaging readouts are optimized to generate a suppressed CSF intensity of –0.5 and high contrast between WM and GM. The equation of self-normalization reconstruction is

$$R = real\left(\frac{S_1^* S_2}{|S_1|^2 + |S_2|^2}\right) \quad (1)$$

where S_1 and S_2 are the GRE signal at inversion recovery delays TI1 and TI2, respectively; and the "*" operator is a complex conjugator.

As discussed by O'Brien,[18] the MP2RAGE reconstruction provides a much flatter T_1-weighted image (than the non-reference-corrected MPRAGE), which enables high-consistency gray-white-CSF segmentation. More importantly, however, it is recognized that the self-correcting strategy can be applied to other acquisitions that acquire multiple readout blocks with a common preparation sequence.

In this report we describe the incorporation of a longitudinal T_2 preparation module with a multiblock inversion recovery 3D acquisition to achieve a CSF-suppressed T_2-weighted image for 7T use in the detection of brain pathology. Our preliminary data demonstrate that the proposed sequence MPFLAGRE (magnetization-prepared fluid attenuated gradient echo) achieves this goal. The sequence uses an inversion recovery with a T_2 spin-echo preparation and multiple short gradient-echo imaging blocks, with the self-correcting normalization[17] generating the calculated MPFLAGRE image. Cerebrospinal fluid suppression is achieved through appropriate timing of TI for T_1 weighting. In this report, we show Bloch simulations to examine the sequence's dependence on T_1 and T_2 and demonstrate its performance with a transceiver array at 7 T. Because of the longitudinal T_2 preparation that is performed with conventional adiabatic refocusing pulses, this sequence efficiently generates whole-brain T_1 and T_2-weighted coverage in single sequence that is well within SAR guidelines.

2 | THEORY

2.1 | Two-block sequence (MPFLAGRE-2)

To generate T_2 FLAIR contrast, our method introduces T_2 weighting into the T_1-weighted MP2RAGE sequence using a longitudinal T_2 encoding module performed after the initial inversion (Figure 1). The T_2 weighting is performed with a nonselective spin-echo module (90_{x+}-180_y -180_y -90_{x-} of duration TE) and is followed by multiple short 3D gradient-echo (readout) blocks. The MPFLAGRE-2 uses 2 blocks, with the first block performed immediately after the spin echo, block S_1. Another signal block, S_2, is performed at another timepoint in the T_1 recovery, which with increasing delay from the S_1 block, reflects primarily T_1 weighting. Equations (2) and (3) give the expressions for the signal for the 2-block sequence:

$$S_1 \propto M_0 e^{-te_g/T_2^*} B_1^- \sin\alpha_1 \left[\left(\frac{e^{\frac{-te}{T2}+\frac{-ti1}{T1}} * \varepsilon M_{ss}}{M0} + \left(1 - e^{\frac{-ti1}{T1}}\right)\right) * A_1^{Ncenter} + R_1^{Ncenter}\right] \quad (2)$$

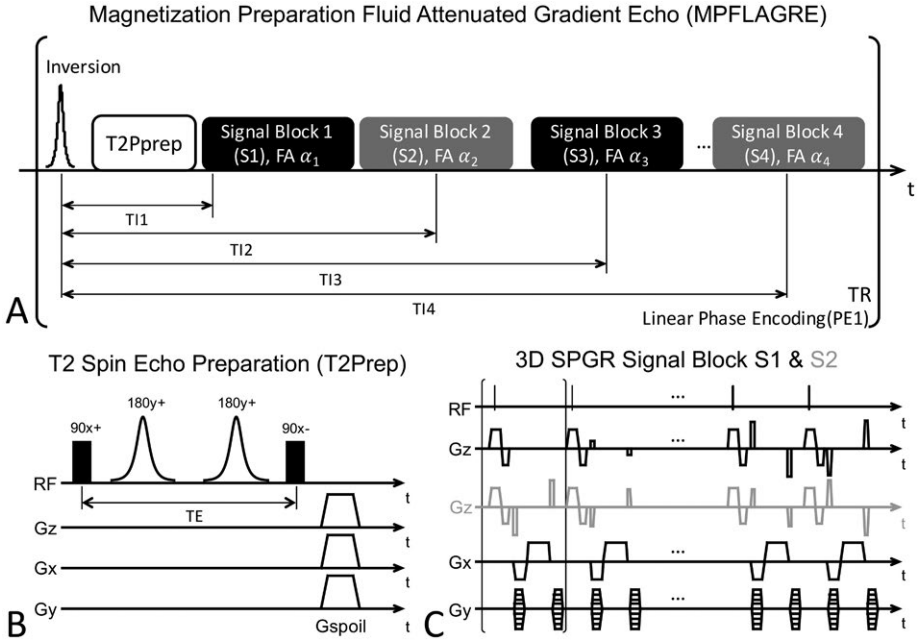

FIGURE 1 Pulse sequence showing the overall sequence (A), T_2 spin-echo module (B), and readout block (C). The MPFLAGRE (magnetization-prepared fluid-attenuated inversion recovery gradient-echo) sequence is able to run with 2, 3, or 4 spoiled gradient blocks. In (C), the readout block is shown either as a centric out (S_1) or a linearly (S_2) encoded coverage

$$S_2 \propto M_0 e^{-te_g/T_2^*} B_1^- sin\alpha_2 \left\{ \begin{array}{c} \left[\left(1-e^{\frac{-ti2}{T1}}+e^{\frac{-ti2}{T1}}R_1^N\right)+e^{\frac{-te}{T2}+\frac{-ti2}{Ti}} * A_1^N\left(1-e^{\frac{-ti1}{T1}}-\frac{M_{ss}}{M0}\varepsilon * e^{\frac{-ti1}{T1}}\right)\right] \\ * A_2^{Ncenter} + R_2^{Ncenter} \end{array} \right\} \quad (3)$$

where $R_{1\,or\,2}^{Npts} = \left(1-e^{\frac{-tr}{T1}}\right)\frac{1-\left(cos(\alpha_{1\,or\,2})e^{-trT1}\right)^{Npts}}{1-cos(\alpha_{1\,or\,2})e^{-trT1}}$; and $A_{1\,or\,2}^{Npts} = \left(cos\left(\alpha_{1\,or\,2}\right)e^{-trT1}\right)^{Npts}$,

where tr is the echo spacing; ε is efficiency of inversion; N is the resolution; ti1 is the delay for block 1; ti2 is the succeeding delay for block 2; te_g is the TE for a single gradient echo; M_{ss} is the steady-state magnetization at the start of each inversion recovery; and M_0 is the total available magnetization signal. Inspection of Eqs. (2) and (3) shows that, as expected, S_1 is weighted strongly by T_2 (center term with $e^{-te/T2}$; with a very short ti1, there is minimal T_1 recovery). Whereas S_2 demonstrates the T_1 recovery due to ti2 (center term $1-e^{-ti2/T1}$), the T_2 effect dissipates with increasing ti2. To combine these images, we use the self-correcting normalization, $R_{1/2}$ as described by Marques,[17] with the inclusion of sign inversion on the T_2-weighted image S_1, to generate the desired tissue orientation (Eq. 3) as follows:

$$R_{1/2} = real\left(\frac{-S_1^* S_2}{|S_1|^2+|S_2|^2}\right). \quad (4)$$

The normalization from Eq. (4) for the 2 signals gives a high 0.5 value when the 2 input intensities, S_1 and S_2, are equal and of opposite sign, and a lesser value when the intensities are unequal. Thus, CSF suppression can be achieved through appropriate timing for the S_2 block to give a CSF signal intensity that is different from the S_1 block. Figure 2 shows Bloch simulations of the 2-block sequence performed over the T_1, T_2 parameter space. For comparison, simulation of the MP2RAGE is shown in Figure 2A using timings of ti1/ti2/TR = 0.9/2.6/5 seconds and tip angles of 5° and 9°. As expected from the MP2RAGE, the base images (S_1 and S_2) and the calculated intensity $R_{1/2}$ (from Eq. 1) is primarily dependent on the T_1 with minimal T_2 dependence (a small dependence results from the finite duration of the adiabatic inversion pulse).

In comparison, Figure 2B shows simulations of the MPFLAGRE-2 sequence, including the T_2 preparation module applied early in the T_1 recovery and using a parameter set of ti1/ti2/TR/TE = 0.1/1.6/5/0.085 seconds and tip angles of 5° and 9°. The calculated image (Eq. 4) shows that the CSF signal (T_1, T_2) taken at [4.3, 0.9] seconds[19] is partially suppressed with $R_{1/2}^{CSF}$ ~-0.18, which is substantially lower than normal $R_{1/2}^{GM}$ and $R_{1/2}^{WM}R_{WM}$. (The T_1, T_2 values for tissue components used in these simulations are CSF = 4.3 seconds, 0.9 seconds; GM = 2.0 seconds, 60 ms; WM = 1.2 seconds, 60 ms.[19-21]) It should be stated that the strategy for MPFLAGRE can also be applied with the spin-echo application applied late (rather than early) in the T_1 recovery. Although there are differences between the early or late T_2 preparation (Supporting Information Figure S3), the strategy remains similar (i.e., to optimize the timings of the T_2 and T_1 weighted blocks used with

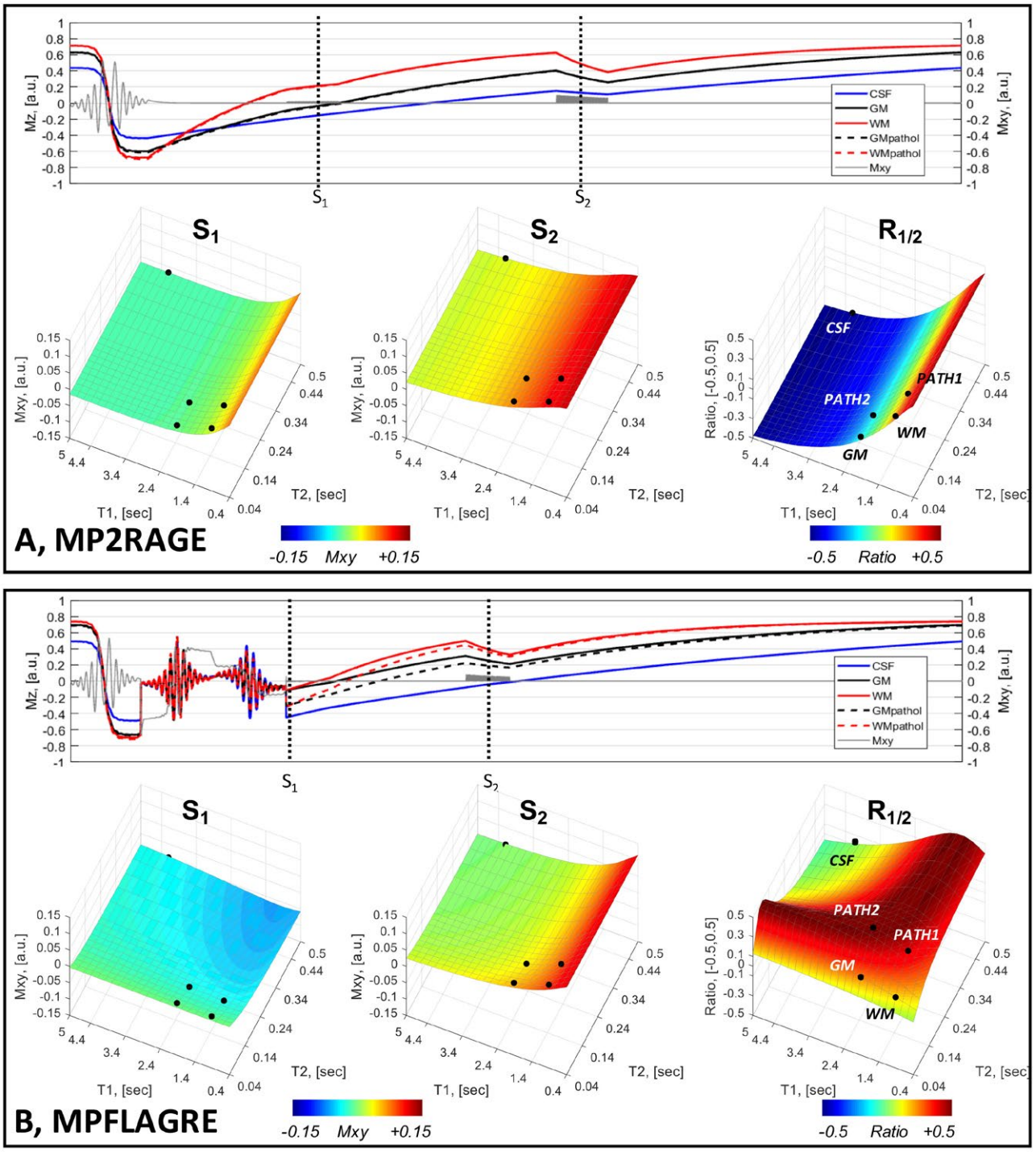

FIGURE 2 Bloch simulations of a 2-block acquisition, S_1 and S_2. A, Using MP2RAGE parameters (i.e., without a T_2 spin-echo preparation). B, MPFLAGRE-2 sequence with T_2 preparation applied early in the inversion recovery. In both (A) and (B), the time course of Iz amplitudes is shown (5 tissue components: blue, CSF; black, gray matter [GM]; red, white matter [WM] with inversion, pathologic T_2). Note that the time axis is not linear, with each unit representing a simulation step. The surface plots of the signal amplitudes are shown over the [T_1, T_2] parameter space for S_1, S_2, and the calculated signal $R_{1/2}$ (using Eqs. (1) and (4). The MP2RAGE sequence (A) shows only the T_1 dependence, whereas the MPFLAGRE-2 sequence (B) shows the effect of the T_2 preparation and T_1. The calculated $R_{1/2}$ shows the CSF suppression and signal detection over the pathologic range of T_2. The black dots on the surface plots indicate the 5 tissue components. The T_1 and T_2 values for CSF are assigned at 4.3 seconds, 0.9 seconds; GM at 2.0 seconds, 60 ms; and WM at 1.2 seconds, 60 ms[19-21]

the self-normalization to achieve CSF suppression due to T_1 differences while maintaining T_2 sensitivity). This report focuses on the T_2 weighting applied early in the T_1 recovery.

2.2 | Three-block and 4-block sequences (MPFLAGRE-3 and MPFLAGRE-4)

The use of multiple readout blocks of acquisition in combination with both T_1 and T_2 preparation in the MPFLAGRE sequence provides additional flexibility. Two aspects of the multiple-block acquisition are considered. First, although the MPFLAGRE-2 sequence is able to suppress CSF, Figure 2B shows that there is relatively limited dynamic range for the calculated $R_{1/2}$ image. To increase this sensitivity with T_2, we recognize that the T_2 preparation induces a change in the longitudinal magnetization and thus the rate of T_1 recovery. Given the typically slow T_1 recovery, the T_2-dependent effects on amplitude and T_1 recovery rate thus transiently persist after the spin echo. To maximize the effect of the spin echo, we can then acquire an additional signal block (Figures 1 and 3A) and sum the 2 succeeding image blocks, S_1 and S_2. Analytically, this can be expressed as a sum of Eqs. (2) and (3), with simplifications including the small values for ti2, ti1, identical tip angles α for S_1 and S_2 (see Eqs. (2) and (3) for other terms, omitting the B_1^-, tip angles, density, and T_2^* factors), and extracting the TE dependent terms:

$$S_1+S_2 \propto -e^{-te/T2}\frac{\varepsilon * M_{ss}}{M0}e^{-ti1/T1}A^{N/2} * \left(1+e^{-ti2/T1}A^{N}\right)+f\left(M_{ss},A^{N},R^{N}\right). \quad (5)$$

With this sign inversion to maintain the desired tissue sensitivity, a third (delayed) block S_3 is then used as the reference image for the self-correcting normalization according to Eq. (6):

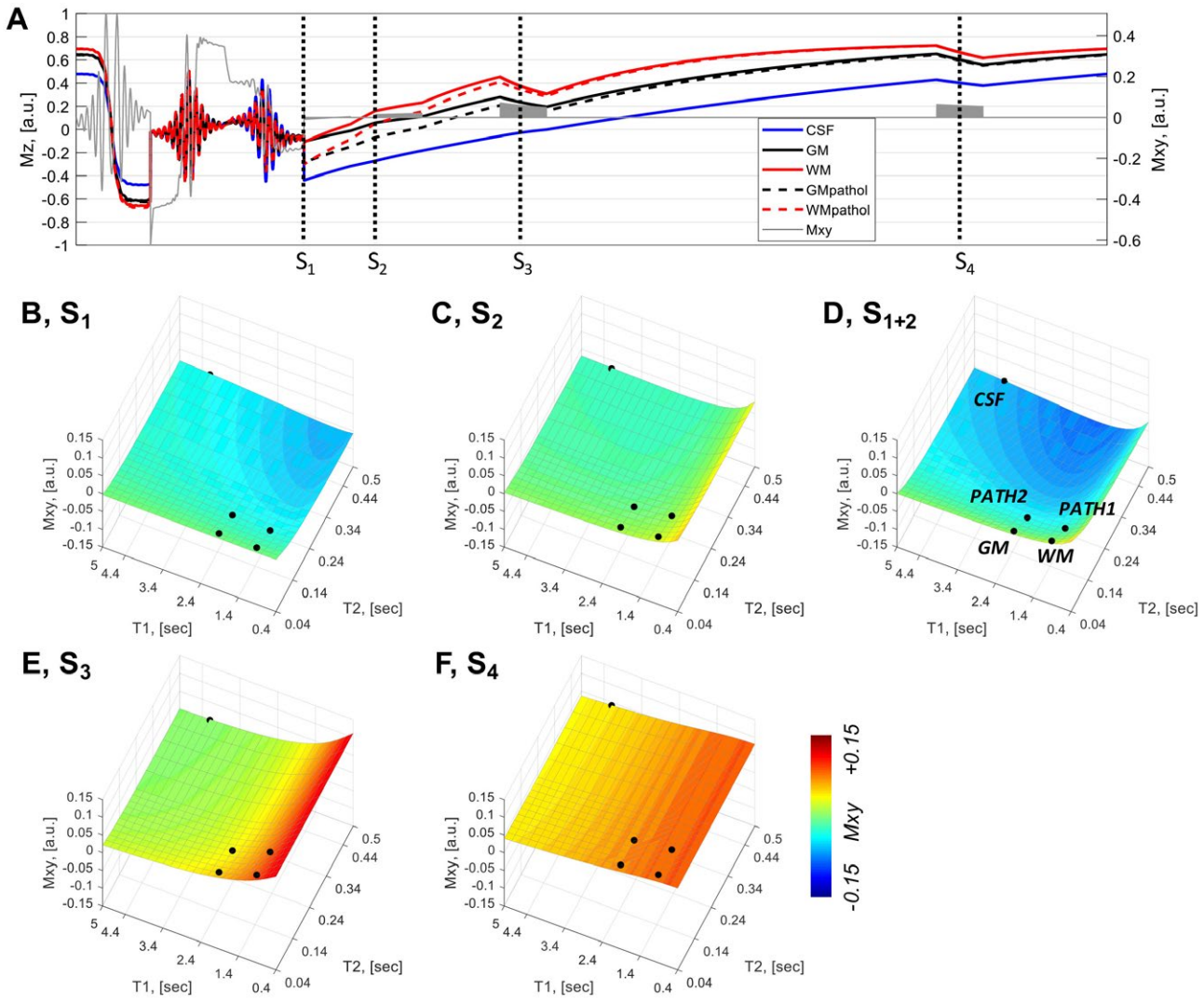

FIGURE 3 Bloch simulations of a 4-block acquisition. A, Time course of Iz amplitudes (5 tissue components: blue, CSF; black, GM; red, WM; GM and WM with long T_2 values for pathology). The [T1, T2] values for CSF are assigned at 4.3 seconds, 0.9 seconds; GM at 2.0 seconds, 60 ms; and WM at 1.2 seconds, 60 ms. B, Signal block 1 intensity is strongly T_2 weighted, shown over the T_1, T_2 parameter space. C, Signal block 2 intensity. D, Summed signal blocks 1+2 show the combined T_1 and T_2 sensitivity. E,F, Signal blocks 3 and 4 are strongly influenced by T_1. All signal intensities are plotted on a scale of [–0.1, 0.1]

$$R_{(1+2)/3} = real\left(\frac{-(S_1+S_2)^* S_3}{|S_1+S_2|^2+|S_3|^2}\right). \quad (6)$$

As seen from Eq. (5) and simulated in Figures 3B-D, the summed block S_{1+2} increases the weighting of the $-e^{-te/T2}$ term from 1 to $1+e^{-ti2/T1}A^N$. Consistent with this, simulation of the summed block strategy shows that the increase in dynamic range for the $R_{(1+2)/3}$ image arises from a drop in the calculated signal for normal tissue, whereas the pathologic long T_2 values "saturate" at 0.5 (Figure 4). Thus, the persistence of the spin-echo effect is a function of T_1 (WM returns more rapidly than GM) (i.e., $R_{(1+2)/3}$ depends on the T_1, as $R^{GM,normal}_{(1+2)/3}$ is larger [brighter] than $R^{WM,normal}_{(1+2)/3}$). With the adjacent block sum of S_1 and S_2, given the same numerical T_2 range is present between normal and pathology for WM and GM (approximately 60 ms to 160 ms), the absolute increase in calculated intensity between normal to pathologic T_2 values is similar between WM and GM: $R^{GM,normal}_{(1+2)/3} - R^{GM,pathol}_{(1+2)/3}$ and $R^{WM,normal}_{(1+2)/3} - R^{WM,pathol}_{(1+2)/3}$.

The second aspect of multiple-block acquisitions arises from the timing and use of the delayed reference image (e.g., through the addition of a fourth imaging block S_4) (Figure 4). Combining the S_1 and S_4 images using Eq. (4) generates a calculated $R_{1/4}$ that, by virtue of their common T_1 factors, largely eliminates T_1 dependence to generate a solely T_2-weighted image (which can be estimated from the simple 2-block analysis in Eqs. and under the conditions of long ti2 and short ti1). For completeness, we also show the calculated $R_{(1+2)/4}$; similar to $R_{(1+2)/3}$, this shows an enhanced dynamic range over T_2 but with mild T_1 sensitivity. Figure 4 shows the resulting simulation, including the calculated $R_{1/3}$ and $R_{(1+2)/3}$ (CSF-suppressed, T_2-weighted) and $R_{1/4}$ and $R_{(1+2)/4}$ (T_2-weighted) images.

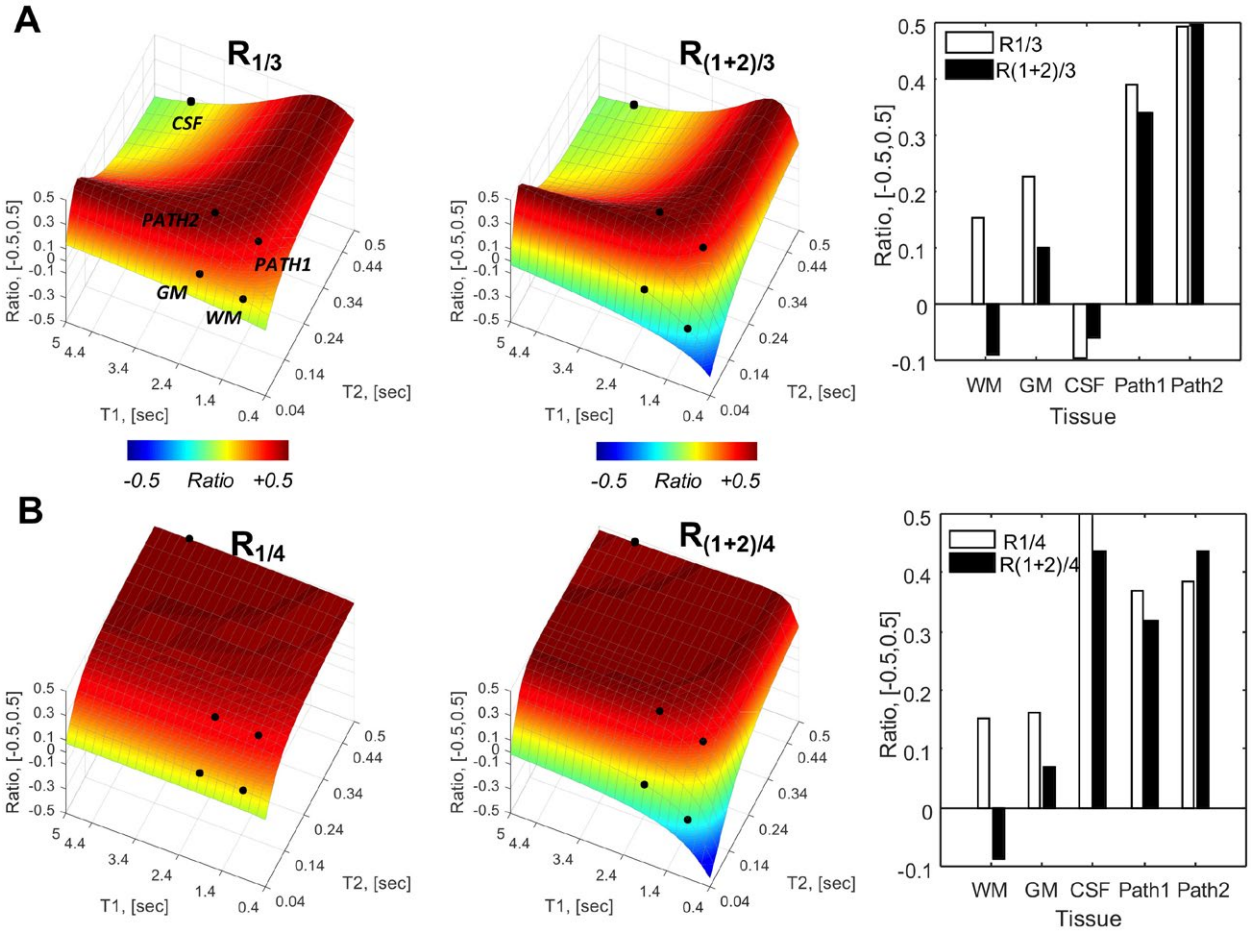

FIGURE 4 Bloch simulations for the MPFLAGRE-4 sequence, adding a delayed S_4 block. See Figure 3A for the time course. Behavior of 5 tissue components identified CSF (blue), GM (black), and WM (red); and GM and WM with long T_2 values for pathology. Calculated R intensities are shown: $R_{1/3}$ and $R_{(1+2)/3}$ intensities as a function of T_1, T_2 space (A) and plots of signal amplitude from the 5 tissue points (far right). B, The $R_{1/4}$ and $R_{(1+2)/4}$ intensities. The $R_{1/3}$, $R_{(1+2)/3}$ amplitudes show CSF suppression and increased amplitudes over long T_2 components. The $R_{1/4}$ amplitude shows predominantly T_2 dependence. The $R_{(1+2)/4}$ intensity, similar to $R_{(1+2)/3}$, shows a larger dynamic range for T_2 dependence

2.3 | B_1^+ dependence

Although the self-correcting normalization eliminates B_1^- variation, variation in B_1^+ is not wholly corrected. Figure 5 considers the B_1^+ dependence of the sequence when multiple acquisition blocks are used to calculate the signal. The transceiver array exhibits 15% SD over the brain when combined with RF shimming (Supporting Information).[6] Simulation results from a MPFLAGRE-4 sequence are shown over the range of T_2 values, using B_1^+ values at ± 15% and ±30% of the optimum B_1^+ value used (750 Hz). The CSF shows the greatest effect with B_1^+ variation, although the R^{CSF} intensity remains at or below the normal-tissue WM intensity R^{WM}. Normal GM and WM show increased R^{GM} and R^{WM}, increasing by less than or equal to 25%. However, it should be noted that in the range of normal T_2 values for GM and WM (40 ms-70 ms[20,21]), the calculated intensity is steeply rising with T_2, and that within a 15% erroneous B_1^+, a less than 10-ms T_2 increase will give the same R^{GM} intensity (i.e., the same signal intensity is equivalent to less than a 10-ms T_2 rise).

2.4 | Pathologic T_2 values

As the goal of the FLAIR sequence is to detect tissues with long (and likely pathologic) T_2 values, we need to have the values of pathologic relaxation at 7 T to properly optimize the parameters of the MPFLAGRE sequence. Although such values have not been widely reported, a 3T estimate is available,[22] which found a less than 20% increase in hippocampal T_2 in epilepsy versus control. We estimate that to leave adequate "head room" for pathology, the calculated image values for normal GM and WM tissue need to be less than 0.30, with CSF intensities at or below the normal tissue values; these values were achieved in these optimizations.

3 | METHODS

We used a Siemens whole-body 7T Magnetom 8-channel multiple transmit system with body gradient coil and an 8 *x* 2 transceiver array for all acquisitions. All studies were approved by the institutional review board. The transceiver array was driven in coil pairs using 8 one-to-two splitters such that coils at equivalent azimuthal positions from the 2 rows are driven by the same RF transmit channel, with independent reception from all 16 channels. A fixed phase shift between the 2 rows is used to ensure constructive addition of the RF across rows and to maximize spatial coverage. B_1 shimming was performed in all subjects, requiring about 3.5 minutes (including 2.5 minutes of B_1 mapping acquisitions).

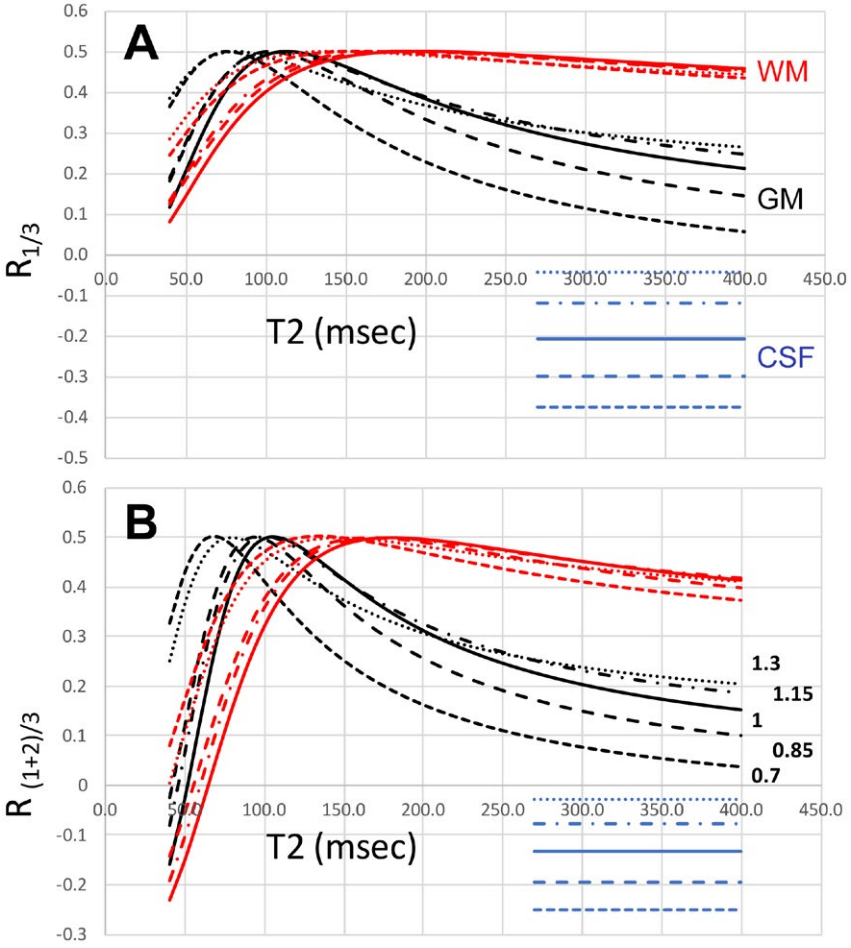

FIGURE 5 B_1^+ influence on MPFLAGRE-4 as a function T_2. A fixed T_1 value is used for GM (2.0 seconds, black) and WM (1.2 seconds, red). The CSF is a single value plotted (4.3 seconds T_1, 0.9 seconds T_2, blue). The range of B_1^+ is 0.70 to 1.30, optimum at 1.0. A, Calculated intensity $R_{1/3}$. B, Calculated intensity $R_{(1+2)/3}$. Consistent with the surface plots in Figure 4, the dynamic range of $R_{(1+2)/3}$ is larger than $R_{1/2}$ by more than 50%. Based on the transceiver range of ±15% (dashed lines), the B_1^+ sensitivity of GM and WM is within approximately 25% over a T_2 range of 60-160 ms

In control subjects, a mean B_1^+ of 17.6 uT with a SD of 10.4 ± 1.8% over the brain using a maximum voltage for every RF channel of less than 170 V (n = 8 subjects[6]; Supporting Information Figures S1 and S2). As a result, conventional pulses are used, including hyperbolic secant pulses with mu = 10 and 4 time constants. With a single T_2 preparation in the MPFLAGRE-4 acquisition and 2π refocusing pulses, the acquisition has a global SAR of 74 ± 2% of the US Food and Drug Administration's guidelines of 3.2 W/kg (using 5 kg for adult head mass), as determined from the Siemens calibrated directional coupler measurements. A total of 5 control subjects were studied (Table 1), with mean height and weight of 62.1 ± 11 kg and 168.1 ± 8.1 cm (3 males, 2 females). A GRAPPA factor of 3 was used, achieving a 0.7 × 0.7 × 1.2 mm (nominal volume 0.6 mm^3) resolution, with an acquisition time of 9.5 minutes. The phase encoding for the imaging blocks were either linear or center out, with the latter used to maintain maximal T_2 weighting at the center of k-space. All timings are thus reported as the duration between the center of the inversion recovery to the k-space center acquisition.

4 | RESULTS

4.1 | MPFLAGRE-2

Figure 6 shows the data acquired from a healthy control using the MPFLAGRE-2 sequence. For comparison, Figure 6A,B shows the data without and with the T_2 preparation, respectively. The timings in Figure 6A are set to create MP2RAGE-like contrast (ti1/ti2/TR = 0.9/2.67/5 seconds, tip angle = 5° and 9°), and as expected, the acquired and calculated images are all strongly T_1 weighted. Figure 6B,C shows the MPFLAGRE-2 data, acquired with ti1/ti2/TR/TE = 0.14/1.65/5/0.100 seconds using pulse angles of 5° and 9°. Figure 6C shows the base images with T_2 contrast dominating the S_1 image. In S_1, the WM-GM contrast is small; this is due to the dynamic range of the signal intensity governed by the high proton density CSF signal and the small WM-GM variation in T_2 at 7 T. Consistent with simulation, there is little T_2 contrast in the CSF-suppressed $R_{1/2}$ image (Figure 6B).

4.2 | MPFLAGRE-4

As the MPFLAGRE-3 acquisition is very similar to that of MPFLAGRE-4, Figure 7 shows the data from the MPFLAGRE-4 sequence. Shown are both the CSF-suppressed (Figure 7A) and T_2-weighted (Figure 7B) calculated images, over a range of [–0.5, 0.5]. The T_2-weighted images $R_{1/4}$ and $R_{(1+2)/4}$ again show the limited dynamic range of T_2 variation at 7 T between WM and GM. The difference between the calculated $R_{1/3}$ and $R_{(1+2)/3}$ images (showing the increase in dynamic range in total signal) is consistent with the simulation, and is a result of decreased calculated signal in normal WM and GM in $R_{(1+2)/3}$. With this effect being different between WM and GM, the $R_{(1+2)/3}$ images show slightly more GM-WM contrast in comparison with $R_{1/3}$. Although this initial report is not intended to evaluate pathology, Figure 8 shows the performance of the MPFLAGRE-4 (same acquisition parameters as in control from Figure 7) in 2 patients (epilepsy, left neocortical temporal lobe, anaplastic astrocytoma). In comparison to a clinical 3T FLAIR (Figure 8C), the epilepsy patient shows bright signal in the lateral cortex and hippocampus consistent with clinical data. The tumor patient shows that the bright MPFLAGRE signal in the temporal lobe extends into the posterior thalamus. The 3T studies were performed on a GE Signal Discovery MR750, with an inversion recovery for the epilepsy T_1 image; T_1 optimized fast spin echo for the tumor T_1 image; and both FLAIRs acquired with 2D fast spin echoes (TR/TI/TE = 11.6 seconds/2.5 seconds/154 ms, resolution = 0.43 × 0.43 × 3.3 mm^3 [epilepsy] and TR = 8.7 seconds/2.2 seconds/150 ms, resolution = 0.63 × 0.63 × 5 mm^3 [tumor]).

4.3 | Comparison with 3D SPACE and contrast-to-noise ratio

For whole-brain coverage, the MPFLAGRE sequence is compared with the 3D variable flip angle SPACE acquisition. As reported by Visser,[10] the SPACE acquisition benefits substantially from 2D acceleration (2.5 × 2.5) but still requires a long TR. Our implementation used a GRAPPA factor of 4; however, a TR of 10 seconds was needed to reduce SAR to within the US Food and Drug

TABLE 1 Signal-to-noise ratio, contrast-to-noise ratio, and SAR for the MPFLAGRE sequence

	SNR			CNR		SAR (FDA max. 15 W)
	GM	WM	CSF	GM-CSF	WM-CSF	
3D SPACE	8.6	12.0	5.6	0.20	4.21	11.6 W (77%)
3D MPFLAGRE-4 $R_{1/3}$	13.7	30.4	7.0	6.17	8.00	10.7 W (70%)
3D MPFLAGRE-4 $R_{1/3}$, N=5	17.0 ± 2.3	35.2 ± 6.1	5.4 ± 18	6.63 ± 1.0	6.94 ± 1.0	11.1 ± 0.5 W (74%)

Abbreviations: CNR, contrast-to-noise ratio; FDA, US Food and Drug Administration.

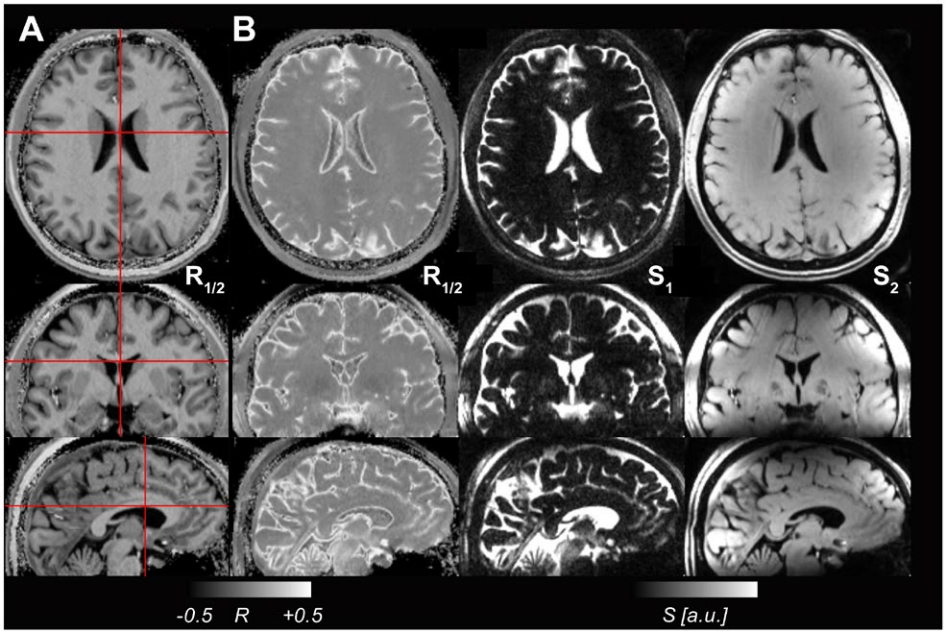

FIGURE 6 Images from a control acquired without a spin-echo preparation with parameters selected to create (A) an MP2RAGE-like image with CSF nulling and bright WM and (B) the MPFLAGRE-2 $R_{1/2}$ image, acquired with a spin-echo TE of 100ms. The individual signal blocks S_1 and S_2 are also shown in (B) for the MPFLAGRE contrast, with image S_1 being heavily T_2 weighted. Image S_2 acquired later is heavily T_1 weighted. For the MPFLAGRE image in (B), the $R_{1/2}$ image shows CSF suppression with relatively weak discrimination between WM and GM, as seen from simulation

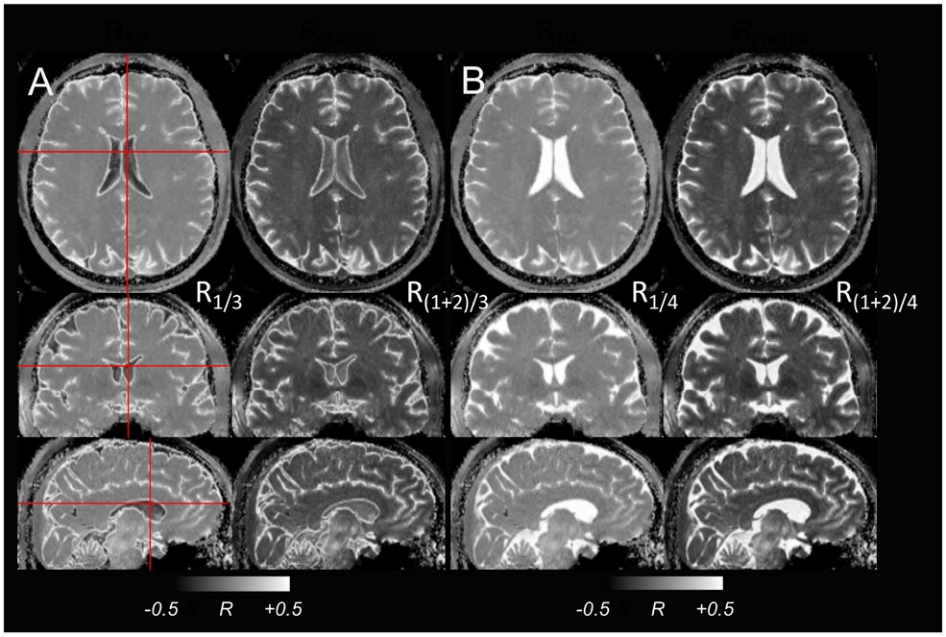

FIGURE 7 The MPFLAGRE-4 data from healthy control. A, Suppressed CSF, showing the 3D view of $R_{1/3}$ and $R_{(1+2)/3}$ images. B, T_2-weighted image showing a 3D view of $R_{1/4}$, and calculated $R_{(1+2)/4}$ image. All gray scaling is shown at [–0.5, 0.5]

Administration's guidelines, resulting in an acquisition of 19.7 minutes with TR/TI/TE of 10.1 seconds/2.35 seconds/200 ms. Figure 9 shows the mildly brighter GM, characteristic of the residual T_1 weighting. However, this contrast is B_1^+-sensitive, and the consistency of the image intensity is relatively poor, reflecting the variation in B_1^- (and B_1^+). Matched in resolution ($0.7 \times 0.7 \times 1.2$ mm^3) with the MPFLAGRE, Table 1 provides the contrast-to-noise ratio (CNR) and SNR between the SPACE and $R_{1/3}$ images for a single volunteer (single session). For region of

interest measurements, contiguous 4 × 4 × 1 pixel blocks were taken from the centrum semi-ovale, thalamus, and posterior ventricle for WM, GM, and CSF. The CNR and SNR were calculated in 5 healthy volunteers (Table 1) using the following equation:

$$CNR = \frac{(R_a - R_b)}{\sqrt{(\sigma_a^2 + \sigma_b^2)/2}}, SNR = \frac{R_a}{\sigma_a}. \quad (7)$$

5 | DISCUSSION

5.1 | T_1 and T_2 dependence of the MPFLAGRE signal

As shown in simulation and implementation, the MPFLAGRE sequence is able to generate T_2-weighted images with controlled T_1 effects. The data show that the T_2 preparation is effective and the self-correcting normalization with multiple

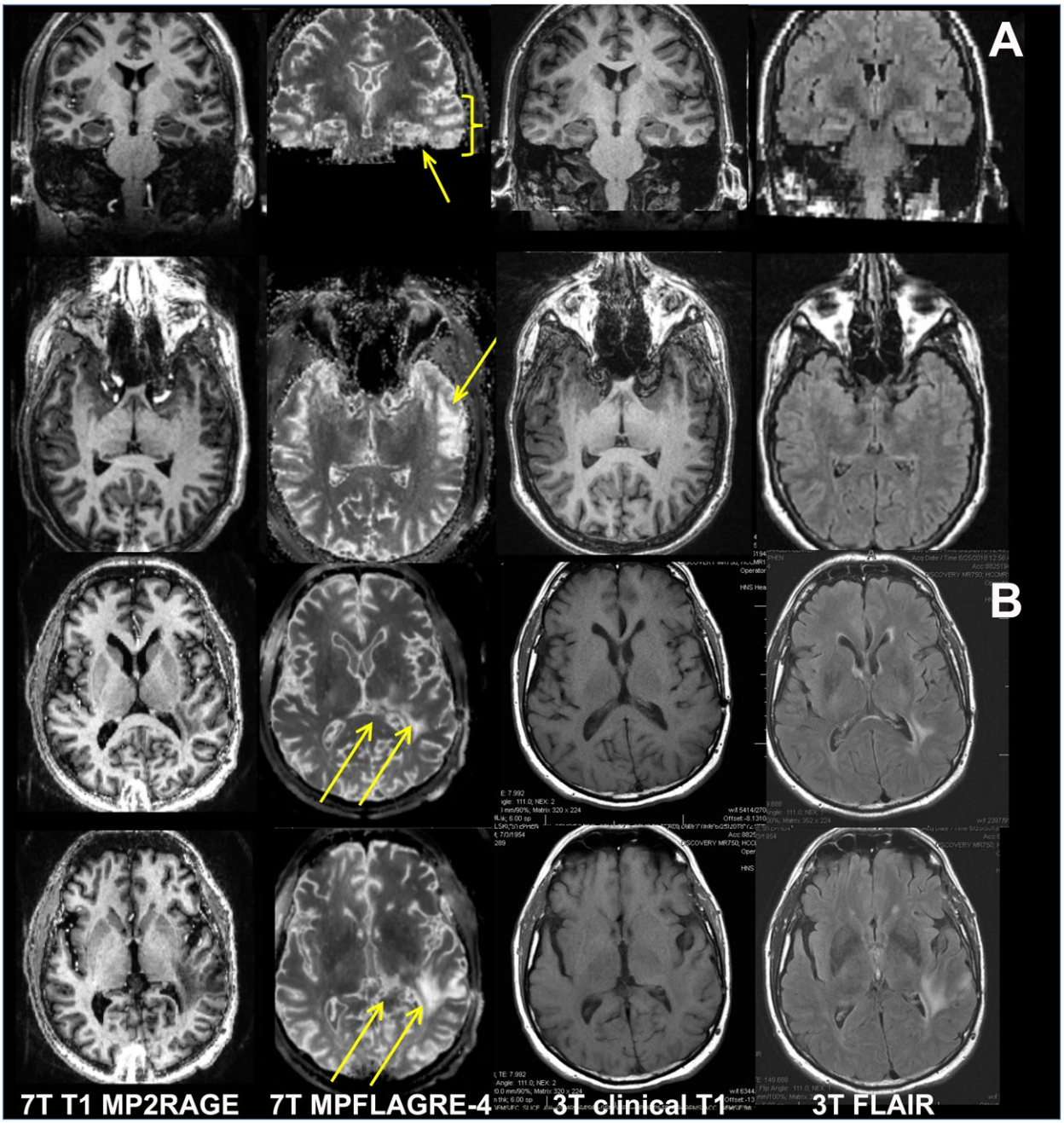

FIGURE 8 Data from an epilepsy (A) and brain tumor patient (B). For both, the coregistered 7T MP2RAGE, MPFLAGRE-4 ($S_{(1+2)/3}$), 3T clinical T_1, and FLAIR images are shown. For the epilepsy patient, increased signal intensity is identified in the lateral left temporal lobe (thick arrows, axial and coronal) and is consistent with clinical data. Note from the coronal image that there is also increased signal in the left hippocampus (thin arrow, coronal), which is characteristic of the local network involvement in temporal lobe epilepsy. The 3T FLAIR from this patient, acquired within 3 months of the 7T images, was interpreted as negative. For the tumor patient, all 7T and 3T images were acquired within 1 week. The arrows identify the increased MPFLAGRE signal in the left temporal lobe extending into the posterior thalamus

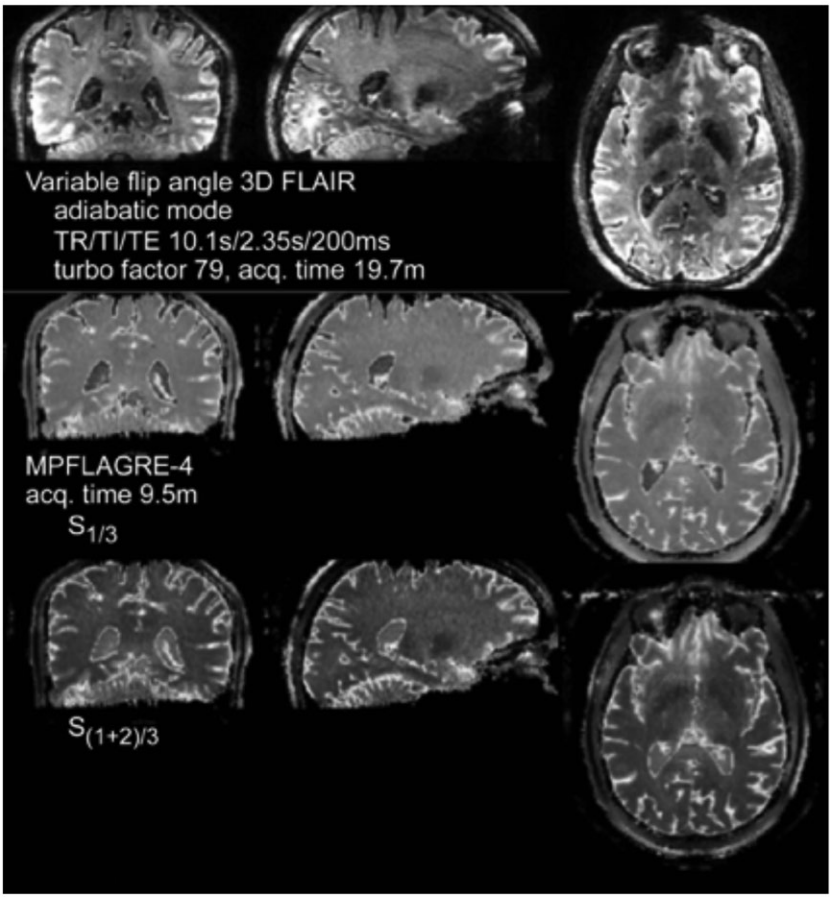

FIGURE 9 Comparison of 3D SPACE (top) with $R_{1/3}$ (middle) and $R_{(1+2)/3}$ (bottom) MPFLAGRE-4 single volunteer in a single session

acquisition blocks enables modulation of the T_1 relaxation effects. The T_1 and T_2 behavior is better understood by recognizing the balance between the T_2-weighted S_1 and reference (non-T_2-weighted) images used in the normalization. In the case in which the common T_1 relaxation factor contributes to both S_1 and the reference image (e.g., S_4 in the MPFLAGRE-4), the normalization results in negligible T_1 dependence regardless of the T_2 value (Figure 4D).

However, if the reference image S_4 is acquired with some residual T_2 (in addition to T_1) weighting, the normalization cannot cancel the T_1 weighting over all T_2 values. Tissues with very long T_2 will be transparent to the spin-echo weighting, and generate a T_1-weighted image. Tissues with extremely short T_2 will approach 0.0 for all T_1 values. Signal from tissues with intermediate relaxation values will vary depending on the specific acquisition parameters and the relaxation values, and thus is a target for optimization. As discussed, suppressing CSF is achieved by optimizing the timings of the 2 blocks (either S_1 and S_2 in MPFLAGRE-2 or S_1 and S_3 in MPFLAGRE-3 and MPFLAGRE-4) to acquire substantially dissimilar signal intensities, ideally generating a signal in the 0 to –0.5 range. With lesional imaging, the goal is to generate significant calculated $R_{T2w,Ref}$ difference between normal and longer (pathologic) T_2 values. Applying the T_2 weighting before the T_1 recovery null, we recognize that pathologic T_2 values will result in "less T_1 later shift" than tissues with normal T_2 values. Thus, to generate an increase in calculated signal from tissue with pathology, the reference image needs to be acquired after the null, sign inverted and larger in absolute amplitude compared with normal T_2 values (i.e., as exemplified with the MPFLAGRE-2 timing).

The limited dynamic range of the 2-block acquisition arises from the amplitudes of signal in the T_2-weighted and reference images. With the MPFLAGRE-3 and MPFLAGRE-4, we expand this range and take advantage of the temporal persistence of the T_2-dependent T_1 later shift effect through the summation of the 2 adjacent blocks. This later shift effect is larger for shorter T_2 components (i.e., normal T_2) rather than pathologic T_2 values (Figure 3). Thus, the sign-sensitive summation of 2 adjacent blocks after the spin echo will result in an apparent decrease in amplitude for normal T_2 components and give decreased $R_{(1+2)/3}$, whereas the pathologic long T_2 components effectively saturate with $R_{(1+2)/3}$ at 0.5. With the shorter T_1 of normal WM, the R^{WM} falls more than R^{GM}. However, because of the similar T_2 values of WM and GM at 7 T, the absolute increases in $R^{GM,normal}_{(1+2)/3} - R^{GM,pathol}_{(1+2)/3}$ and $R^{WM,normal}_{(1+2)/3} - R^{WM,pathol}_{(1+2)/3}$ are similar for both tissues; this effect is also seen with the simpler MPFLAGRE-2 sequence.

5.2 | Specific absorption rate and CNR of the MPFLAGRE sequence

From a SAR perspective, the use of a single nonselective adiabatic spin echo allows the MPFLAGRE sequence to function with high efficiency. With the MPFLAGRE-4 sequence, over n = 5 adult control volunteers, the 6-minute average SAR was maintained at 74% ± 2% of the US Food and Drug Administration's guidelines. The CNR between WM-GM is approximately 1.0 (data not shown), which is consistent with the small differences in their T_2 at 7 T. For GM-CSF the CNR is 6.63 ± 1.0, and for WM-CSF the CNR is 6.94 ± 1.0, which again is consistent with the similar intensities between WM and GM. In spite of the combination of multiple images used in this approach, which may otherwise be expected to increase variability, the coefficient of variance(s) in the MPFLAGRE data are comparatively low at less than 15%, reflecting their nonrandom source of variability.[17] As a result, the SNR and CNR are higher with the MPFLAGRE sequence in comparison with the variable flip angle acquisition.

Inspection of Figures 5 and 6 show that there is enhanced signal intensity at the cortical rim and ependyma. This is consistent with the report of von Veluw,[23] who concluded that increased T_2 contributes to their enhanced FLAIR signal intensity. Although quantitative T_2 data do not exist on these tissue components, a long T_2 for the cortical rim is not surprising, given that it contains the comparatively poorly vascularized molecular layer I of the neocortex. Similarly, the high signal intensity from the ependyma is likely related to its function as the neuroepithelial layer around the ventricle that contributes to the production and regulation of CSF.

5.3 | Caveats with the MPFLAGRE sequence

The primary challenge with this sequence is its B_1^+ sensitivity, as shown in Figure 9. A 15% increase or decrease in B_1^+ results in increased intensity $R_{1/3}$ by less than 20% for WM and less than 28% for GM, although this effect decreases at longer T_2. However, this effect arises from the steep rise of R over the normal range of T_2 values. From a viewpoint of a given $R_{1/3}$ intensity, a 15% B_1^+ variation results in a small decline in apparent T_2 by about 10 ms for GM (about 5 ms for white matter). With 30% B_1^+ inhomogeneity, these effects increase substantially, with the T_2 sensitivity curves broadly shifting to lower T_2 values (i.e., there can be erroneously bright signal [> 0.30] for relatively normal T_2 values). In practice, our experience with the transceiver with the adiabatic refocusing pulses has not been shown to be a major problem for this over the entire head. Nonetheless, this sensitivity can be improved with incorporation of an adiabatic excitation spin-echo module, such as that used by Dyvorne and Balchandani,[16] although at added SAR cost.

With the CSF suppression generated from the normalization strategy performed between the multiple acquisition blocks, acquisition of differing resolution images but at the same delay times can change the resulting contrast. However, for the given parameters there is excellent consistency between different subjects, as indicated in Table 1 and the patient data. Nonetheless, this effect can be minimized with use of additional acceleration methods in 2 or 3 dimensions. In addition, magnetization-transfer effects, which are not modeled here, can differentially affect the signal between the $S_{i,j}$ blocks and thus contribute to the contrast.[24] Notably, with magnetization-transfer effects typically decreasing the signal intensity in high-density (normal) tissue, this would result in an enhancement of the apparent MPFLAGRE sensitivity to pathology (the pathologic longer T_2 would exhibit a lesser magnetization-transfer effect). Finally, the need for relatively long TR still limits the entire acquisition at approximately 10 minutes. However, with generation of both the T_2 and CSF-suppressed T_2-weighted images in a single matched image, the MPFLAGRE remains an efficient acquisition.

6 | CONCLUSIONS

In summary, we have developed and demonstrated the MPFLAGRE sequence as a flexible acquisition that builds on the self-correcting normalization strategy[17] to generate T_2 and CSF-suppressed T_2 weighted contrast at 7 T. This is performed by incorporating a longitudinal spin-echo weighting within the context of an inversion recovery. With appropriate timing and combination of multiple imaging blocks during the inversion recovery, it is possible to control the T_1 dependence and specifically suppress CSF. Not surprisingly, the T_2-weighted image, even when corrected for M_0, B_1^- and T_2^*, displays relatively little contrast between WM and GM, reflecting the small to minimal difference in T_2 at 7 T. As applied with a transceiver array, the sequence functions well within SAR guidelines. Overall, as the CSF-suppressed T_2-weighted contrast is designed for sensitivity to pathology, additional work with patients will be necessary to further optimize the parameters at 7 T.

ACKNOWLEDGMENTS

This work was supported by NIH R01EB011639, R01NS090417, and R01NS081772. The authors would like to thank Professor Robert Turner for pointing out the potential magnetization-transfer effect in this acquisition.

REFERENCES

1. Uğurbil K. The road to functional imaging and ultrahigh fields. *NeuroImage*. 2012;62:726–735.
2. Ivanov D, Poser BA, Huber L, Pfeuffer J, Uludağ K. Optimization of simultaneous multislice EPI for concurrent functional perfusion and BOLD signal measurements at 7T. *Magn Reson Med*. 2017;78:121–129.
3. Moser E, Stahlberg F, Ladd ME, Trattnig S. 7-T MR—from research to clinical applications? *NMR Biomed*. 2012;25:695–716.
4. Tallantyre EC, Morgan PS, Dixon JE, et al. A comparison of 3T and 7T in the detection of small parenchymal veins within MS lesions. *Invest Radiol*. 2009;44:491–494.
5. Pittau F, Baud MO, Jorge J, et al. MP2RAGE and susceptibility-weighted imaging in lesional epilepsy at 7T. *J Neuroimaging*. 2018;28:365–369.
6. Hetherington H, Zhao T, Starewicz P, Pan JW. RF shimming approaches for 7T multi-row transceiver arrays. In: Proceedings of the 10th Biennial High and Ultra-High Field MR Imaging Workshop, Minneapolis, MN; 2015.
7. Vaughan JT, Garwood M, Collins CM, et al. 7T vs. 4T: RF power, homogeneity, and signal-to-noise comparison in head images. *Magn Reson Med*. 2001;46:24–30.
8. Eggenschwiler F, O'Brien KR, Gruetter R, Marques JP. Improving T2 -weighted imaging at high field through the use of kT -points. *Magn Reson Med*. 2014;71:1478–1488.
9. Setsompop K, Alagappan V, Zelinski AC, et al. High-flip-angle slice-selective parallel RF transmission with 8 channels at 7 T. *J Magn Reson*. 2008;195:76–84.
10. Visser F, Zwanenburg JJ. Hoogduin JM, Luijten PR. High-resolution magnetization-prepared 3D-FLAIR imaging at 7.0 Tesla. *Magn Reson Med*. 2010;64:194–202.
11. Busse RF, Hariharan H, Vu A, Brittain JH. Fast spin echo sequences with very long echo trains: design of variable refocusing flip angle schedules and generation of clinical T2 contrast. *Magn Reson Med*. 2006;55:1030–1037.
12. Cloos MA, Boulant N, Luong M, et al. kT -points: short three-dimensional tailored RF pulses for flip-angle homogenization over an extended volume. *Magn Reson Med*. 2012;67:72–80.
13. Haase A. Snapshot FLASH MRI. Applications to T1, T2, and chemical-shift imaging. *Magn Reson Med*. 1990;13:77–89.
14. Mugler J, Spraggins T, Brookeman J. T2 weighted 3-dimentional MP-RAGE MR imaging. *J Mag Res Imaging*. 1991;1:731–737.
15. Parrish T, Hu X. A new T2 preparation technique for ultrafast gradient echo sequence. *Magn Res Med*. 1994;32:652–657.
16. Dyvorne H, Balchandani P. Slice-selective adiabatic magnetization T_2 -preparation (SAMPA) for efficient T_2 -weighted imaging at ultrahigh field strengths. *Magn Reson Med*. 2016;76:1741–1749.
17. Marques J, Kober T, Krueger G, et al. MP2RAGE, a self bias-field corrected sequence for improved segmentation and T1 mapping at high field. *NeuroImage*. 2010;49:1271–1281.
18. O'Brien KR, Kober T, Hagmann P, et al. Robust T1-weighted structural brain imaging and morphometry at 7T using MP2RAGE. *PLoS ONE*. 2014;9:e99676.
19. Rooney WD, Johnson G, Li X, et al. Magnetic field and tissue dependencies of human brain longitudinal 1H2O relaxation in vivo. *Magn Reson Med*. 2007;57:308–318.
20. Michaeli S, Garwood M, Zhu XH, et al. Proton T2 relaxation study of water, N-acetylaspartate, and creatine in human brain using Hahn and Carr-Purcell spin echoes at 4T and 7T. *Magn Reson Med*. 2002;47:629–633.
21. Daoust A, Dodd S, Nair G, et al. Transverse relaxation of cerebrospinal fluid depends on glucose concentration. *Magn Reson Imaging*. 2017;44:72–81.
22. Briellmann RS, Syngeniotis A, Fleming S, Kalnins RM, Abbott DF, Jackson GD. Increased anterior temporal lobe T2 times in cases of hippocampal sclerosis: a multi-echo T2 relaxometry study at 3 T. *Am J Neuroradiol*. 2004;25:389–394.
23. van Veluw SJ, Fracasso A, Visser F, et al. FLAIR images at 7 Tesla MRI highlight the ependyma and the outer layers of the cerebral cortex. *NeuroImage*. 2015;104:100–109.
24. Rioux JA, Levesque IR, Rutt BK. Biexponential longitudinal relaxation in white matter: characterization and impact on T1 mapping with IR-FSE and MP2RAGE. *Magn Reson Med*. 2016;75:2265–2277.

SUPPORTING INFORMATION

Additional supporting information may be found online in the Supporting Information section at the end of the article.

FIGURE S1 Two configurations are shown for driving the 8×2 transceiver from 8 independent RF channels. In configuration A, a single RF channel drives 2 adjacent coils within a row. In configuration B, a single RF channel drives 2 longitudinally adjacent coils

FIGURE S2 Experimental data showing performance of the 2 configurations. For each configuration, the MP2RAGE and B_1 maps are shown. In configuration B, 2 RF distributions can be defined to excite the "homogeneous" volume and a "ring" volume

FIGURE S3 Bloch simulations of a late T_2 preparation 2-block acquisition, S_1 and S_2. A, The time course of Iz amplitudes is shown (5 tissue components: blue, CSF; black, GM; red, WM with inversion; pathologic T_2). Note that the time axis is not linear, with each unit representing a simulation step. B, The surface plots of the signal amplitudes are shown over the [T_1, T_2] parameter space for S_1, S_2, and the calculated signal $R_{1/2}$ (using Eq. 1). The calculated $R_{1/2}$ shows the CSF suppression and signal enhancement over the pathologic range of T_2. The black dots on the surface plots indicate the 5 tissue components: T_1, T_2 values for CSF are assigned at 4.3 seconds, 0.9 seconds; GM at 2.0 seconds, 60 ms; and WM at 1.2 seconds, 60 ms

How to cite this article: Pan JW, Moon CH, Hetherington HP. Cerebrospinal fluid–suppressed T_2-weighted MR imaging at 7 T for human brain. *Magn Reson Med*. 2019;81:2924–2936. https://doi.org/10.1002/mrm.27598